

## Spectropolarimetric Observations of an Arch Filament System with GREGOR

H. Balthasar,<sup>1</sup> P. Gömöry,<sup>2</sup> S. J. González Manrique,<sup>1,3</sup> C. Kuckein,<sup>1</sup>  
 A. Kučera,<sup>2</sup> P. Schwartz,<sup>2</sup> T. Berkefeld,<sup>4</sup> M. Collados,<sup>5</sup> C. Denker,<sup>1</sup> A. Feller,<sup>6</sup>  
 A. Hofmann,<sup>1</sup> D. Schmidt,<sup>7</sup> W. Schmidt,<sup>4</sup> M. Sobotka,<sup>8</sup> S. K. Solanki,<sup>6,9</sup>  
 D. Soltau,<sup>4</sup> J. Staude,<sup>1</sup> K. G. Strassmeier,<sup>1</sup> and O. von der Lühe<sup>4</sup>

<sup>1</sup>*Leibniz-Institut für Astrophysik Potsdam (AIP), 14482 Potsdam, Germany;  
 hbalthasar@aip.de*

<sup>2</sup>*Astronomical Institute of the Slovak Academy of Sciences, Tatranská  
 Lomnica, Slovak Republic*

<sup>3</sup>*Universität Potsdam, Institut für Physik und Astrophysik, 14476 Potsdam,  
 Germany*

<sup>4</sup>*Kiepenheuer-Institut für Sonnenphysik, 79104 Freiburg, Germany*

<sup>5</sup>*Instituto de Astrofísica de Canarias, 38205 La Laguna (Tenerife), Spain*

<sup>6</sup>*Max-Planck-Institut für Sonnensystemforschung, 37077 Göttingen, Germany*

<sup>7</sup>*National Solar Observatory, Sunspot NM 88349, U.S.A.*

<sup>8</sup>*Astronomical Institute, Academy of Sciences of the Czech Republic, Ondřejov,  
 Czech Republic*

<sup>9</sup>*Kyung Hee University, Yongin, Gyeonggi-Do, 446 701, Republic of Korea*

**Abstract.** We observed an arch filament system (AFS) in a sunspot group with the GREGOR Infrared Spectrograph attached to the GREGOR solar telescope. The AFS was located between the leading sunspot of negative polarity and several pores of positive polarity forming the following part of the sunspot group. We recorded five spectro-polarimetric scans of this region. The spectral range included the spectral lines Si I 1082.7 nm, He I 1083.0 nm, and Ca I 1083.9 nm. In this work we concentrate on the silicon line which is formed in the upper photosphere. The line profiles are inverted with the code ‘Stokes Inversion based on Response functions’ to obtain the magnetic field vector. The line-of-sight velocities are determined independently with a Fourier phase method. Maximum velocities are found close to the ends of AFS fibrils. These maximum values amount to  $2.4 \text{ km s}^{-1}$  next to the pores and to  $4 \text{ km s}^{-1}$  at the sunspot side. Between the following pores, we encounter an area of negative polarity that is decreasing during the five scans. We interpret this by new emerging positive flux in this area canceling out the negative flux. In summary, our findings confirm the scenario that rising magnetic flux tubes cause the AFS.

## 1. Introduction

Arch Filament Systems (AFS) have been described by Howard & Harvey (1964), Martres et al. (1966) and Bruzek (1967, 1969). They appear preferentially in young sunspot groups where magnetic flux is still emerging. The single fibrils of AFSs (visible in chromospheric lines) connect opposite magnetic polarities crossing the ‘Polarity Inversion Line’ (PIL). Moderate upflows are found in the central parts of the fibrils, while strong downflows are detected towards the ends of the fibrils. This scenario is explained by rising flux tubes that transport matter to higher layers in their more or less horizontal parts, and this matter then streams down towards the footpoints of the fibrils (Bruzek 1969). Recently, AFS have been studied with higher spatial resolution and with spectropolarimetry by Solanki et al. (2003), Spadaro et al. (2004), Lagg et al. (2007), Xu et al. (2010), Vargas Domínguez et al. (2012), Grigor’eva et al. (2012), and Ma et al. (2015). A study of the magnetic field in deep photospheric layers and the corresponding velocity field of the same active region considered in the present work has been presented by Balthasar et al. (2016). Similar observations of different active regions are studied by González Manrique et al. (2016) and Verma et al. (2016). Nevertheless it remains an open question how the different layers of the solar atmosphere are connected and where exactly to locate the footpoints of the AFS fibrils in the photosphere. In this work we investigate the upper photosphere using a silicon line.

## 2. Observations and Data Reduction

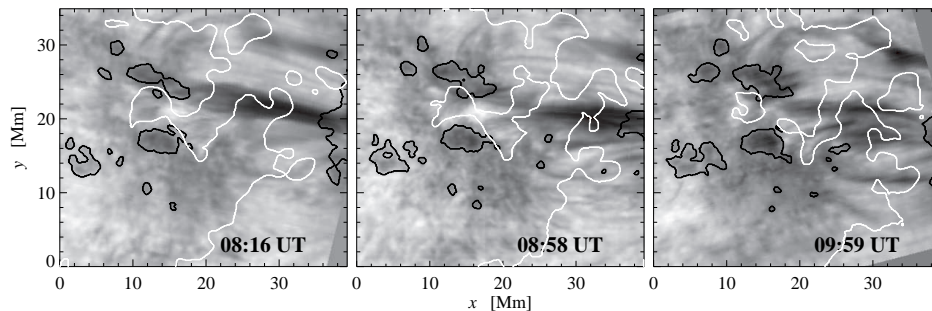


Figure 1. Line-core intensities of the ‘red’ component of the helium line at 1083.0 nm. Black contours outline the pores and a part of the penumbra at the right edge, and the white line indicates the PIL derived from the silicon line.

The following part of active region NOAA 12353 was observed on May 24, 2015 with the GREGOR solar telescope in Tenerife (Schmidt et al. 2012). The images were stabilized with an adaptive optics system (GAOS, Berkefeld et al. 2012). Spectropolarimetric data were obtained with the GREGOR Infrared Spectrograph (GRIS, Collados et al. 2012) which is equipped with the former Tenerife Infrared Polarimeter II (Collados et al. 2007). The observed spectral range included the spectral line Si I 1082.7 nm, the triplet He I 1083.0 nm, and the line Ca I 1083.9 nm. The basic data reduction steps follow the description of Collados (1999), and the polarimetric calibration was performed with the GREGOR polarimetric calibration unit (Hofmann et al. 2012). Within two hours, we took five scans across the region, but because of the page limit we show only

three of them here. More details about these observations are given by Balthasar et al. (2016). Figure 1 displays the line-core intensities in the so-called ‘red’ component of the helium triplet formed in the upper chromosphere. The fibrils of the AFS appear as dark stripes connecting the main spot (outside the scan region except for the outer penumbra) with the area of the following pores.

The profiles of the photospheric lines (Si I 1082.7 nm and Ca I 1083.9 nm) were inverted using the code ‘Stokes Inversion based on Response functions’ (SIR, Ruiz Cobo & del Toro Iniesta 1992). For details of the inversion of the calcium line, we refer to Balthasar et al. (2016). Because the silicon line is sensitive over a wider height range, we set five nodes for temperature in the second and third iteration cycle (instead of three, as used for the calcium line). The magnetic field parameters were kept height independent. The magnetic azimuth ambiguity was resolved in the same way as for the calcium line, and finally, all images have been derotated numerically by applying the method described in the appendix of Balthasar et al. (2016).

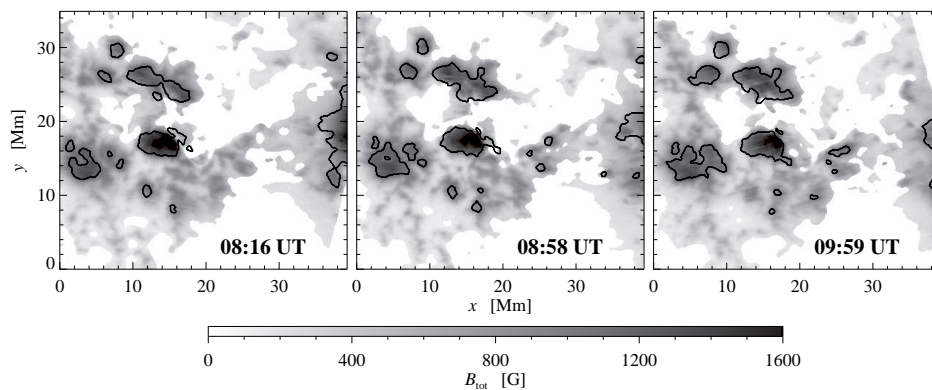


Figure 2. Total magnetic field strength derived from the silicon line. Black contours outline the dark photospheric structures. Values from areas with insignificant polarization signal are suppressed and shown in white.

The Doppler velocities for the silicon line were also obtained from Stokes- $I$  profiles with a Fourier phase method described by Schlichenmaier & Schmidt (2000). This method yields the position of the line profile as a whole. The positions of nearby telluric water vapor lines were used to compensate for shifts caused by the spectrograph. Their mean value in the field-of-view was assumed to be zero.

### 3. Results

The total magnetic field strength is displayed in Fig. 2. The maximum values derived from the silicon line are much lower than those from the calcium line (see Balthasar et al. 2016). Here we encounter only values up to 1600 G, except for the central pore ( $x = 14$  Mm,  $y = 18$  Mm) where the maximum value is 1920 G. This difference with respect to the calcium line is caused by the distinct formation heights of the two spectral lines, the silicon line forming higher than the calcium one. Outside the pores, the polarization signal from the silicon line is stronger, and we detect a magnetic field in a more extended spatial range than for the lower photosphere. In Fig. 3 we show the inclination of the magnetic field in the local reference frame. Values below  $90^\circ$  indicate

a positive polarity which we detect for the pores. The main spot on the right has a negative polarity. Between the pores we find an area with negative polarity. Determined from the silicon line, this area was connected with the main spot, and the fibrils of the AFS lay above this connection, with some of them crossing the winding PIL (see Fig. 1) three times. Such a connection of negative polarity was not detectable for the calcium line (see Balthasar et al. 2016). Next to the pores, this area of negative polarity decreased in size during our observations, as already found for the calcium line (see Balthasar et al. 2016).

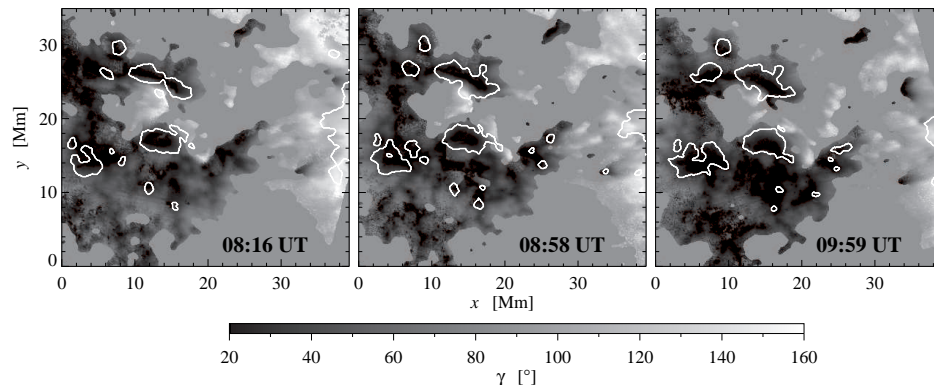


Figure 3. Inclination of the magnetic field derived from the silicon line. White contours outline the dark photospheric structures. Values from areas with insignificant polarization signal are suppressed and shown in medium gray.

The Doppler velocities obtained from the silicon line are displayed in Fig. 4. They exhibit a granular pattern outside the pores, although the contrast is smaller than for the calcium line (due to the higher formation layers). In the region below the AFS fibrils, patches with the same direction of the velocities are somewhat larger than in the quiet Sun, and there is a tendency that strong blueshifts occur preferentially close to the PIL on the side with the positive magnetic polarity of the pores. In the penumbra, we mainly detect redshifts, although one would expect blueshifts according to the photospheric Evershed effect, since the disk center is towards the left in the images. However, the silicon line is formed in the upper photosphere, and therefore it is less sensitive to the Evershed effect which is much stronger in the deep photosphere. In the left panel at 08:16 UT, there is one patch at the boundary of the penumbra of the main spot with a very high redshift of  $4 \text{ km s}^{-1}$  that is likely related to the right end of a dark AFS-fibril. The maximum velocity occurs between the position of the maximum seen in the helium line and that of the calcium line (see Balthasar et al. 2016). Downflows between the two major pores reach  $2.4 \text{ km s}^{-1}$ , structured in several small patches. In one of these patches indicated by arrows in Fig. 4, the downflow turns into an upflow of  $0.8 \text{ km s}^{-1}$ .

#### 4. Discussion and Conclusions

It is difficult to identify photospheric structures that are directly related to the chromospheric structures as seen in the helium line. This holds especially for the footpoints of the fibrils of the AFS. This problem is also pointed out by Schad et al. (2013). While the silicon line probes the upper photosphere up to 500 km the helium line is formed in

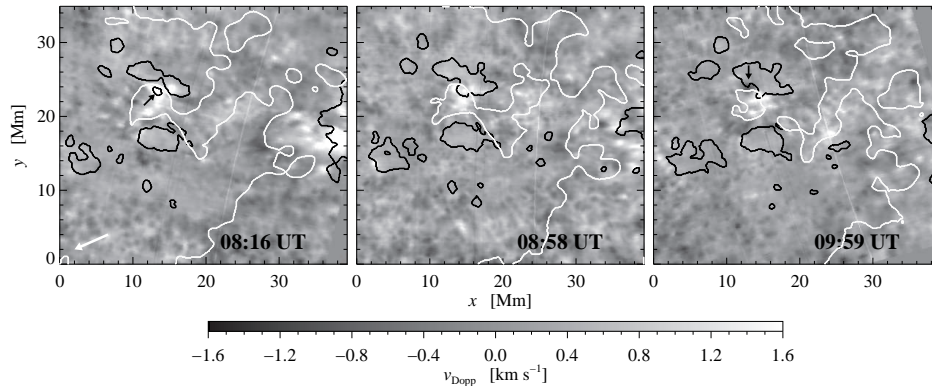


Figure 4. Doppler velocities derived from the silicon line. Black contours outline the dark photospheric structures, and the white contours indicate the PIL. The display is limited to the range  $\pm 1.6 \text{ km s}^{-1}$ . The small black arrows point to a small patch where the sign of the Doppler shifts changed from the first to the last scan. The white arrow points to the disk center.

much higher layers, probably even higher than 1000 km (see e.g., Muglach & Schmidt 2001). Merenda et al. (2011) found that loops in a region with emerging flux reach up to more than 5000 km, and they obtained the best fit for a top height of 6300 km. For a reconstruction of the magnetic field, Xu et al. (2010) assume a loop height of 3000 km. With the present data, we cannot close this gap.

In the scenario of rising flux tubes, one would expect the highest velocities close to the very ends of the fibrils. However, during our first scan we find the highest Doppler velocities from the silicon line just beside the visible ends of the fibrils above the spot. In addition, looking at the positions of highest velocities deduced from the calcium and the helium lines (Balthasar et al. 2016), we find that the highest velocities from the helium line are further to the West than the maximum from the calcium line, and the maximum from the silicon line falls in between. From a simple rising loop scenario one would expect the opposite, but the strong magnetic field of the spot itself is near, and in higher layers where the influence from the sunspot is less, the loop expands for more than the distance of the photospheric footpoints.

Between the pores, we encounter magnetic flux of opposite polarity compared to the positive polarity of the pores. The area of this negative flux decreases during the period of our observations, which we explain by rising magnetic loops. The loops appear first close to the PIL and have the same magnetic orientation as the whole sunspot group. While rising, the small positive footpoints move towards the area between the pores, and field lines reconnect. In an alternative scenario the negative flux is return flux related to the pores and is already connected below the solar surface with the emerging loops. When the loops rise, the magnetic field lines straighten, and the negative polarity is no longer visible.

Our results confirm the scenario of rising flux tubes creating the fibrils of the AFS, as it was proposed by Bruzek (1967, 1969) and confirmed by Xu et al. (2010). Nevertheless, the silicon data show that the real magnetic configuration is more complex than this simple picture. The PIL is winded, and the fibrils of the AFS cross the PIL three

times. Our work to invert the helium line is still in progress, and we shall report on the results in a future article.

**Acknowledgments.** The 1.5-meter GREGOR solar telescope was built by a German consortium under the leadership of the Kiepenheuer-Institut für Sonnenphysik in Freiburg (KIS) with the Leibniz-Institut für Astrophysik Potsdam (AIP), the Institut für Astrophysik Göttingen (IAG), the Max-Planck-Institut für Sonnensystemforschung in Göttingen (MPS), and the Instituto de Astrofísica de Canarias (IAC), and with contributions by the Astronomical Institute of the Academy of Sciences of the Czech Republic (ASCR). SJGM is grateful for financial support from the Leibniz Graduate School for Quantitative Spectroscopy in Astrophysics, a joint project of AIP and the Institute of Physics and Astronomy of the University of Potsdam. This work was supported by a program of the Deutscher Akademischer Austauschdienst (DAAD) and the Slovak Academy of Sciences for project related personnel exchange (project No. 57065721). This work received additional support by project VEGA 2/0004/16. The GREGOR observations were obtained within the SOLARNET Transnational Access and Service (TAS) program, which is supported by the European Commission's FP7 Capacities Program under grant agreement No. 312495.

## References

- Balthasar, H., Gömöry, P., González Manrique, S.J., et al. 2016, AN 337, 1050  
 Berkefeld, T., Schmidt, D., Soltau, D., et al. 2012, AN, 333, 863  
 Bruzek, A. 1967, Solar Phys., 2, 451  
 Bruzek, A. 1969, Solar Phys., 8, 29  
 Collados, M. 1999, in: Third Advances in Solar Physics Euroconference: Magnetic Fields and Oscillations, eds. B. Schmieder, A. Hofmann, & J. Staude, ASPC, 184, 3  
 Collados, M., Lagg, A., Díaz García, J.J. et al. 2007, in: The Physics of Chromospheric Plasmas, eds. P. Heinzel, I. Dorotovič, & Rutten, R.J., ASPC, 368, 611  
 Collados, M., López, R., Páez, E., et al. 2012, AN, 333, 872  
 González Manrique, S.J., Kuckein, C., Pastor Yabar, A., et al. 2016, AN 337, 1057  
 Grigor'eva, I.Y., Shakhovskaya, A.N., Livshits, M.A., & Knyazeva, I.S. 2012, Astron. Rep., 56, 887  
 Hofmann, A., Arlt, K., Balthasar, H., et al. 2012, AN, 333, 854  
 Howard, R. & Harvey, J. 1964, ApJ, 139, 1328  
 Lagg, A., Woch, J., Solanki, S.K., & Krupp, N. 2007, A&A, 462, 1147  
 Ma, L., Zhou, W., Zhou, G. & Zhang, J. 2015, A&A, 583, A110  
 Martres, M.-J., Michard, R., & Soru-Iscovici, I. 1966, Ann. Astrophys., 29, 249  
 Merenda, L., Lagg, A., & Solanki, S. K. 2011, A&A, 532, A63  
 Muglach, K. & Schmidt, W. 2001, A&A, 379, 592  
 Ruiz Cobo, B. & del Toro Iniesta, J.C. 1992, ApJ, 398, 375  
 Schad, T.A., Penn, M., & Lin, H. 2013, ApJ, 768, 111  
 Schlichenmaier, R. & Schmidt, W. 2000, A&A, 358, 1122  
 Schmidt, W., von der Lühe, O., Volkmer, R., et al. 2012, AN, 333, 796  
 Solanki, S.K., Lagg, A., Woch, J., Krupp, N., & Collados, M. 2003, Nature, 425, 692  
 Spadaro, D., Billotta, S., Contarino, L., Romano, P., & Zuccarello, F. 2004, A&A, 425, 309  
 Vargas Domínguez, S., van Driel Gestelyi, L., & Bellot Rubio, L.R. 2012, Solar Phys., 278, 99  
 Verma, M., Denker, C., Böhm, F., et al. 2016, AN, 337, 1090  
 Xu, Z., Lagg, A., & Solanki, S.K. 2010, A&A, 520, A77